Supporting Information

A family of lanthanide compounds with reduced nitronyl nitroxide diradical: syntheses, structures and magnetic properties

Zhao-Xin Xiao,[a] Hao Miao,[a] Dong Shao,[a] Hai-Yan Wei,*[b] Yi-Quan Zhang,*[c] and Xin-Yi Wang*[a]

[a.] *State Key Laboratory of Coordination Chemistry, Collaborative Innovation Center of Advanced Microstructures, School of Chemistry and Chemical Engineering, Nanjing University, Nanjing, 210023, China. E-mail: wangxy66@nju.edu.cn.*

[b.] *Jiangsu Key Laboratory of Biofunctional Materials, School of Chemistry and Materials Science, Nanjing Normal University, Nanjing, 210023, China. Email: weihaiyan@njnu.edu.cn.*

[c.] *Jiangsu Key Laboratory for NSLSCS, School of Physical Science and Technology, Nanjing Normal University, Nanjing 210023, China. E-mail: zhangyiquan@njnu.edu.cn*

1. X-ray crystallography and powder x-ray diffraction

Table S1. Selected bond lengths [Å] and angles [°] for radical **1**.

O(2)-N(2)	1.271(2)	O(1)-N(1)-C(7)	125.85(19)
O(1)-N(1)	1.271(3)	C(7)-N(1)-C(5)	111.28(17)
N(2)-C(7)	1.340(3)	N(3)-C(8)-C(7)	115.00(18)
N(1)-C(7)	1.329(3)	N(1)-C(7)-N(2)	110.57(18)
C(8)-C(7)	1.486(3)	N(1)-C(7)-C(8)	125.62(19)
O(2)-N(2)-C(7)	126.05(17)	N(2)-C(7)-C(8)	123.80(19)

Table S2. Selected bond lengths [Å] and angles [°] for complex $\mathbf{2_{Gd}}$.

Gd(1)-O(4)	2.363(5)	Gd(1)-O(2)	2.473(5)
Gd(1)-O(1)	2.376(4)	Gd(1)-O(8)	2.485(5)
Gd(1)-O(7)	2.383(5)	O(1)-N(1)	1.368(7)
Gd(1)-O(3)	2.389(5)	N(1)-C(19)	1.320(8)
Gd(1)-O(6)	2.432(5)	N(2)-C(19)	1.352(9)
Gd(1)-O(5)	2.444(5)	N(1)-O(1)-Gd(1)	129.5(3)

Table S3. Selected bond lengths [Å] and angles [°] for complex $\mathbf{3_{Dy}}$.

Dy(1)-O(3)	2.314(2)	Dy(1)-O(4)	2.415(2)
Dy(1)-O(1)	2.314(2)	Dy(1)-O(8)	2.421(2)
Dy(1)-O(7)	2.331(2)	O(1)-N(1)	1.357(3)
Dy(1)-O(5)	2.342(2)	N(1)-C(22)	1.291(4)
Dy(1)-O(6)	2.376(2)	N(2)-C(22)	1.341(4)
Dy(1)-O(2)	2.392(2)	N(1)-O(1)-Dy(1)	129.95(16)

Table S4. Selected bond lengths [Å] and angles [°] for complex $\mathbf{4_{Ho}}$.

Ho(1)-O(3)	2.295(4)	Ho(1)-O(4)	2.403(4)
Ho(1)-O(1)	2.304(4)	Ho(1)-O(8)	2.409(4)
Ho(1)-O(7)	2.317(4)	O(1)-N(1)	1.361(5)
Ho(1)-O(5)	2.335(4)	N(1)-C(7)	1.298(7)
Ho(1)-O(6)	2.359(4)	N(2)-C(7)	1.351(7)
Ho(1)-O(2)	2.384(4)	N(1)-O(1)-Ho(1)	129.9(3)

Table S5. Selected bond lengths [Å] and angles [°] for complex $\mathbf{5_{Er}}$.

Er(1)-O(3)	2.286(4)	Er(1)-O(8)	2.402(4)
Er(1)-O(1)	2.291(3)	Er(1)-O(4)	2.403(4)
Er(1)-O(7)	2.306(4)	O(1)-N(1)	1.351(5)
Er(1)-O(5)	2.323(4)	N(1)-C(7)	1.305(6)
Er(1)-O(6)	2.357(4)	N(2)-C(7)	1.342(7)
Er(1)-O(2)	2.369(4)	N(1)-O(1)-Er(1)	129.6(3)

Table S6. Selected bond lengths [Å] and angles [°] for complex $\mathbf{6_{Tm}}$.

Tm(1)-O(1)	2.283(3)	Tm(1)-O(6)	2.395(3)
Tm(1)-O(5)	2.284(4)	Tm(1)-O(8)	2.397(3)
Tm(1)-O(2)	2.298(3)	O(1)-N(1)	1.358(5)
Tm(1)-O(7)	2.313(3)	N(1)-C(22)	1.299(6)
Tm(1)-O(3)	2.353(3)	N(2)-C(22)	1.345(6)
Tm(1)-O(4)	2.372(3)	N(1)-O(1)-Tm(1)	130.0(2)

Table S7. Selected bond lengths [Å] and angles [°] for complex $\mathbf{7_{Yb}}$.

Yb(1)-O(3)	2.269(3)	Yb(1)-O(8)	2.365(3)
Yb(1)-O(1)	2.277(3)	Yb(1)-O(4)	2.374(3)
Yb(1)-O(7)	2.295(3)	O(1)-N(1)	1.351(5)
Yb(1)-O(5)	2.296(3)	N(1)-C(7)	1.296(6)
Yb(1)-O(6)	2.328(3)	N(2)-C(7)	1.348(6)
Yb(1)-O(2)	2.352(3)	N(1)-O(1)-Yb(1)	129.2(2)

Table S8. Lanthanide geometry analysis by using the Shape software for $\mathbf{2_{Gd}}$-$\mathbf{7_{Yb}}$.

Compound / Label	$\mathbf{2_{Gd}}$	$\mathbf{3_{Dy}}$	$\mathbf{4_{Ho}}$	$\mathbf{5_{Er}}$	$\mathbf{6_{Tm}}$	$\mathbf{7_{Yb}}$
OP-8	30.442	30.476	30.448	30.483	30.497	30.219
HPY-8	22.736	22.920	22.968	22.873	22.914	22.927
HBPY-8	15.270	15.444	15.521	15.442	15.547	15.518
CU-8	8.528	8.637	8.717	8.665	8.730	8.606
SAPR-8	1.056	1.050	1.059	1.061	1.070	0.988
TDD-8	1.212	1.158	1.115	1.072	1.050	1.095
JGBF-8	14.833	14.928	14.959	15.150	15.264	15.164
JETBPY-8	28.383	28.541	28.764	28.757	28.757	28.804
JBTP-8	2.252	2.220	2.153	2.172	2.180	2.214
BTPR-8	1.891	1.887	1.873	1.874	1.873	1.893
JSD-8	3.747	3.662	3.560	3.529	3.438	3.615
TT-8	9.164	9.260	9.315	9.280	9.309	9.245
ETBPY-8	23.452	23.779	23.902	23.830	23.990	23.881

Label	Code	Symmetry	Shape
OP-8	1	D8h	Octagon
HPY-8	2	C7v	Heptagonal pyramid
HBPY-8	3	D6h	Hexagonal bipyramid
CU-8	4	Oh	Cube
SAPR-8	5	D4d	Square antiprism
TDD-8	6	D2d	Triangular dodecahedron
JGBF-8	7	D2d	Johnson - Gyrobifastigium (J26)
JETBPY-8	8	D3h	Johnson - Elongated triangular bipyramid (J14)

JBTP-8	9	C2v	Johnson - Biaugmented trigonal prism (J50)
BTPR-8	10	C2v	Biaugmented trigonal prism
JSD-8	11	D2d	Snub disphenoid (J84)
TT-8	12	Td	Triakis tetrahedron
ETBPY-8	13	D3h	Elongated trigonal bipyramid

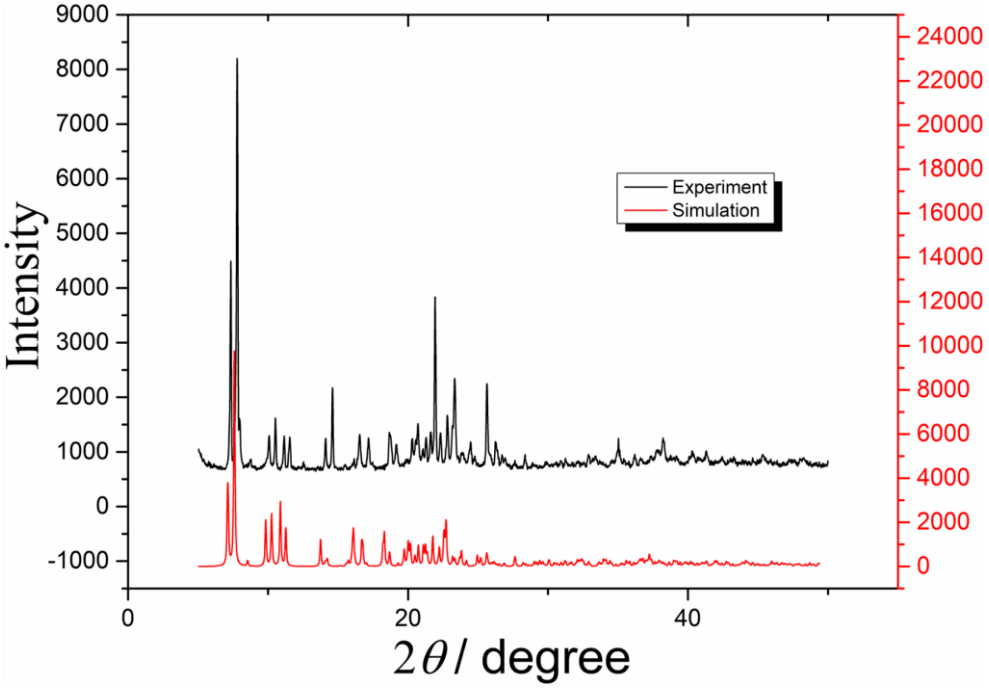

Fig. S1 X-ray powder diffraction pattern of complex $\mathbf{2}_{\mathbf{Gd}}$.

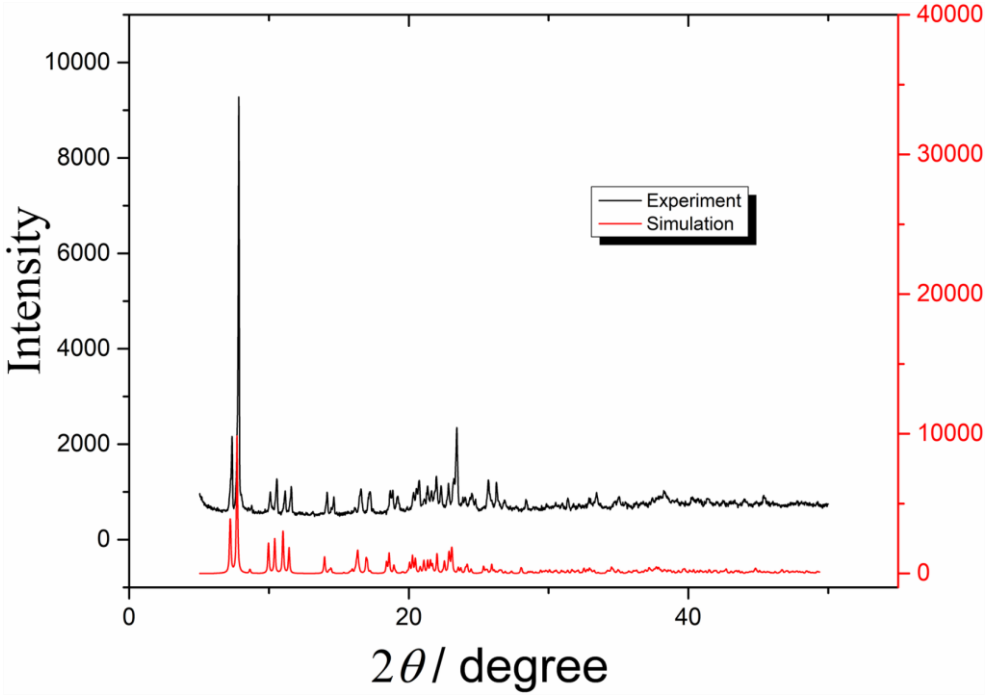

Fig. S2 X-ray powder diffraction pattern of complex $\mathbf{3}_{\mathbf{Dy}}$.

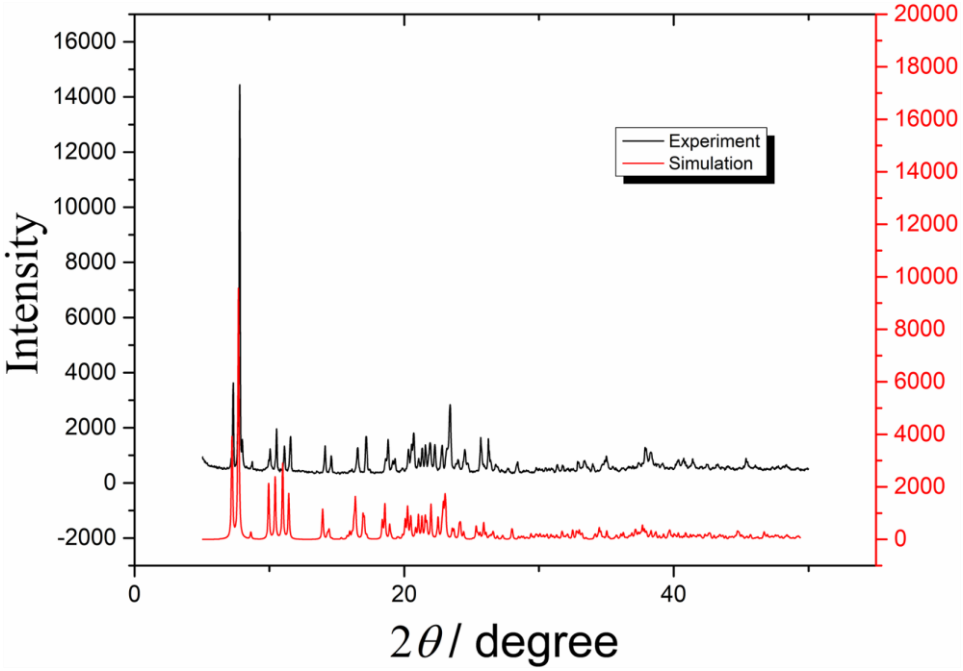

Fig. S3 X-ray powder diffraction pattern of complex $\mathbf{4}_{\mathbf{Ho}}$.

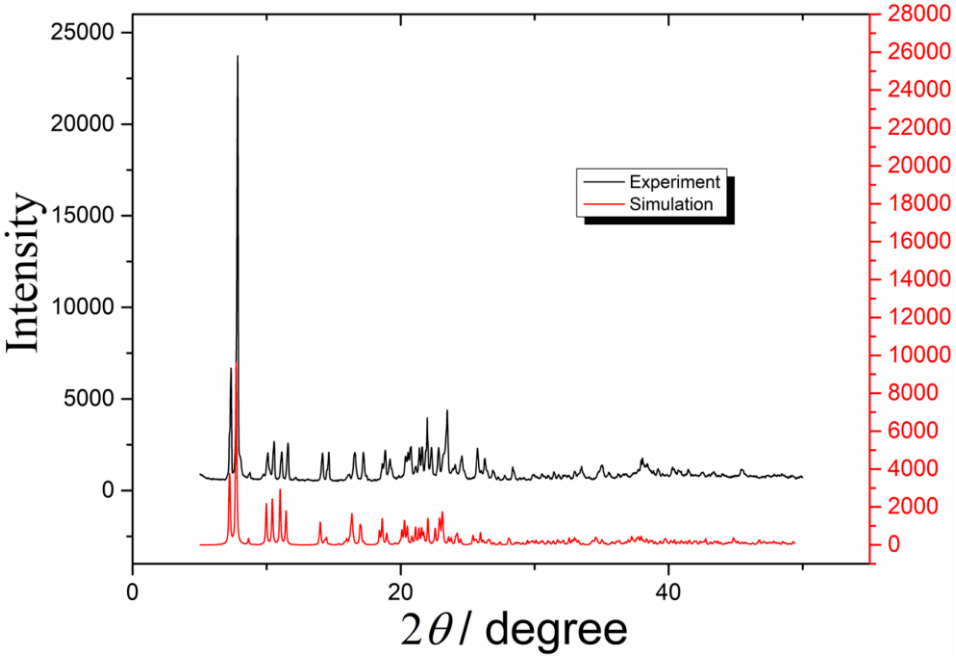

Fig. S4 X-ray powder diffraction pattern of complex $\mathbf{5}_{\mathbf{Er}}$.

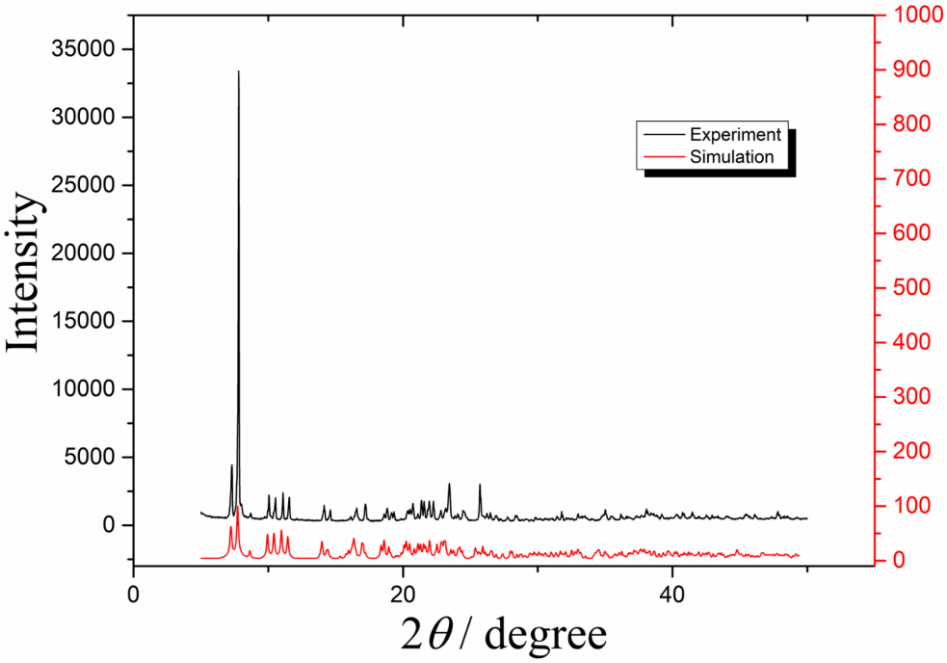

Fig. S5 X-ray powder diffraction pattern of complex $\mathbf{6}_{\mathbf{Tm}}$.

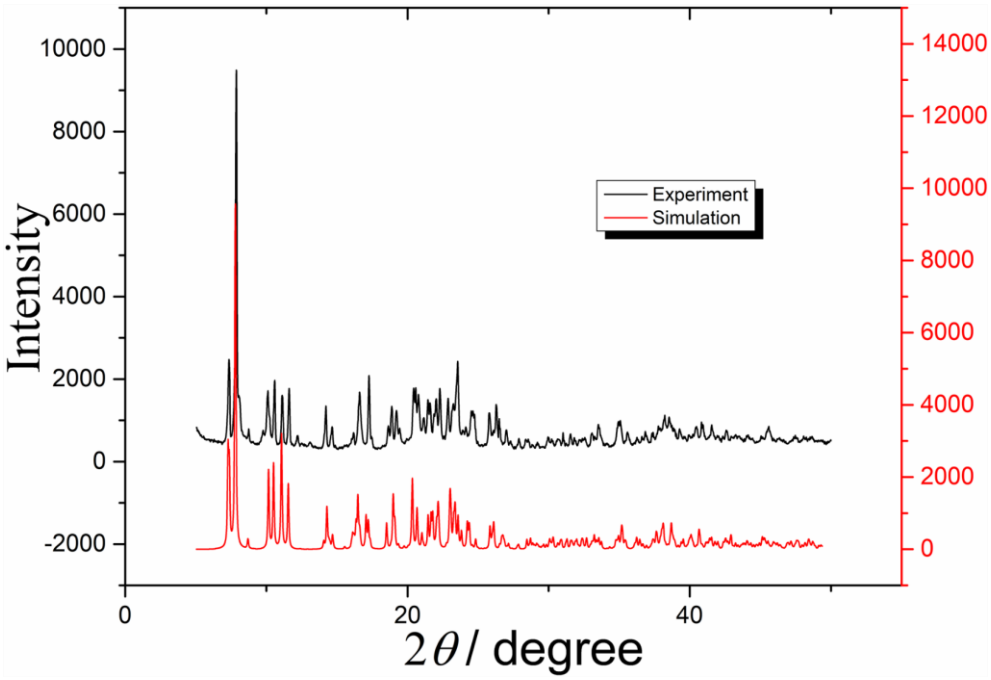

Fig. S6 X-ray powder diffraction pattern of complex $\mathbf{7}_{\mathbf{Yb}}$.

2. Magnetic Properties

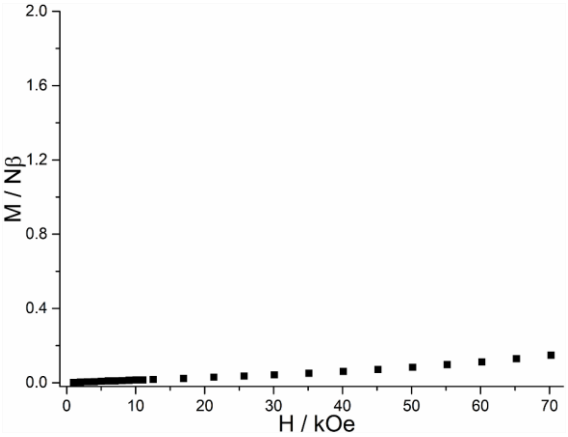

Fig. S7 Field dependent magnetization at 2 K for diradical **1**.

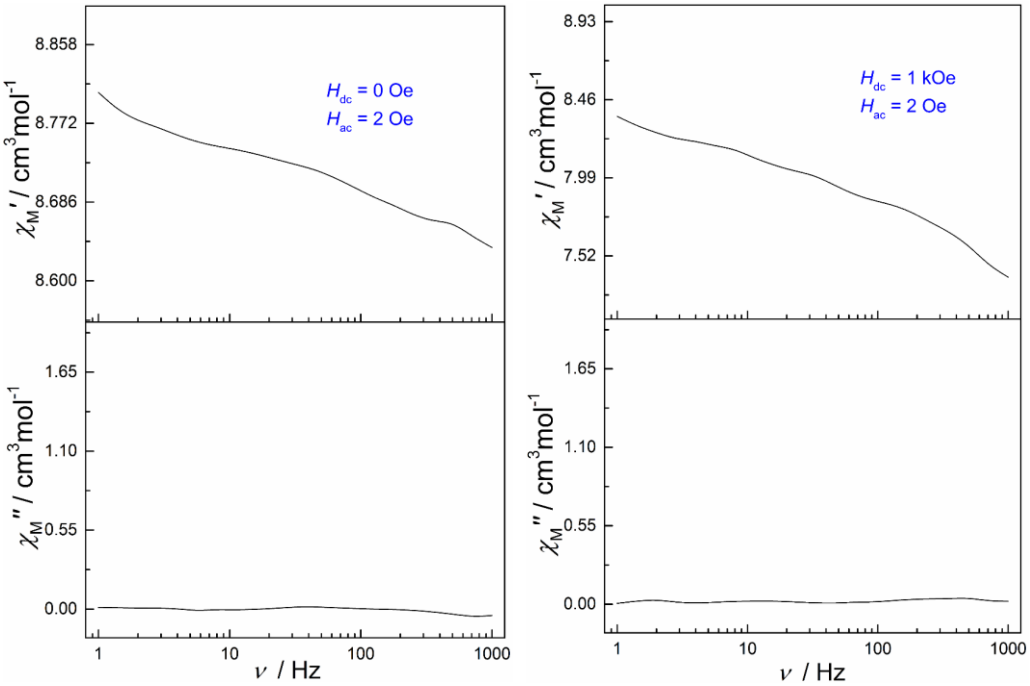

Fig. S8 The real and imaginary components of ac magnetic susceptibilities for $\mathbf{2_{Gd}}$ at 2 K under zero applied external dc field (left) and a dc field of 1000 Oe (right).

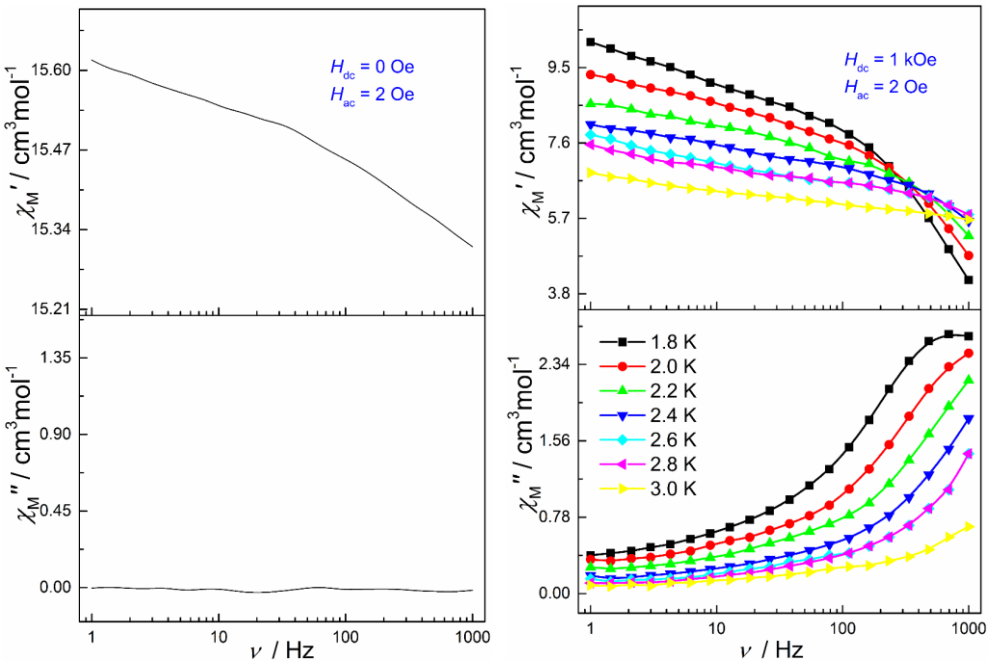

Fig. S9 The real and imaginary components of ac magnetic susceptibility for $\mathbf{3_{Dy}}$ at 2 K under zero applied external dc field (left) and a dc field of 1000 Oe (right).

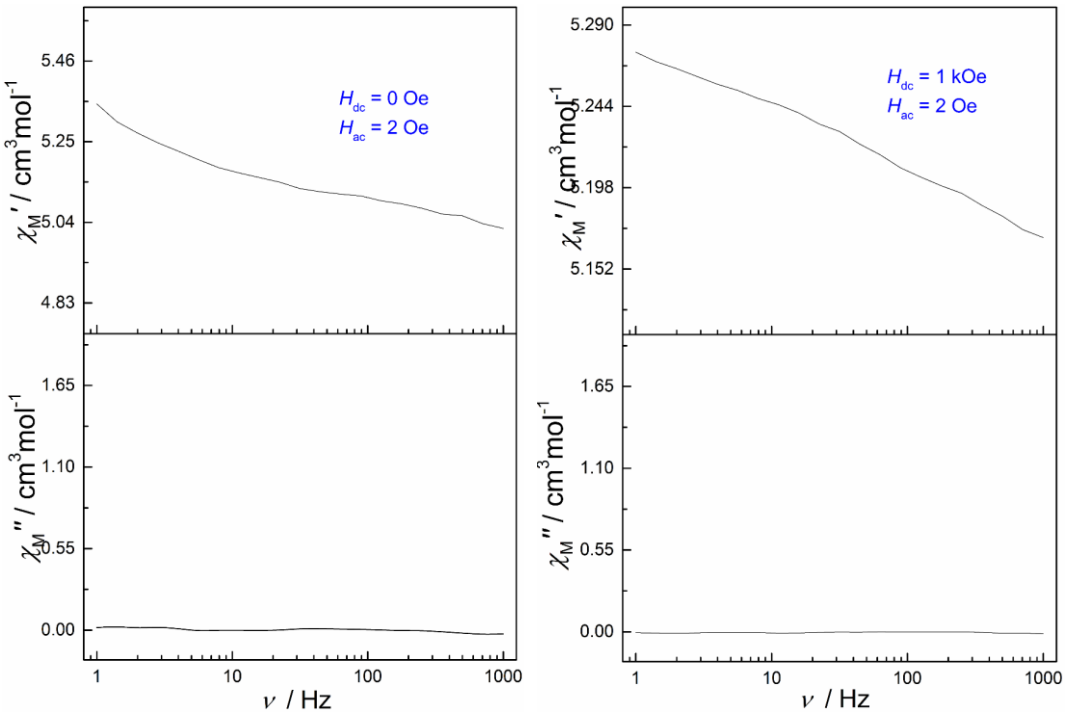

Fig. S10 The real and imaginary components of ac magnetic susceptibility for $\mathbf{4_{Ho}}$ at 2 K under zero applied external dc field (left) and a dc field of 1000 Oe (right).

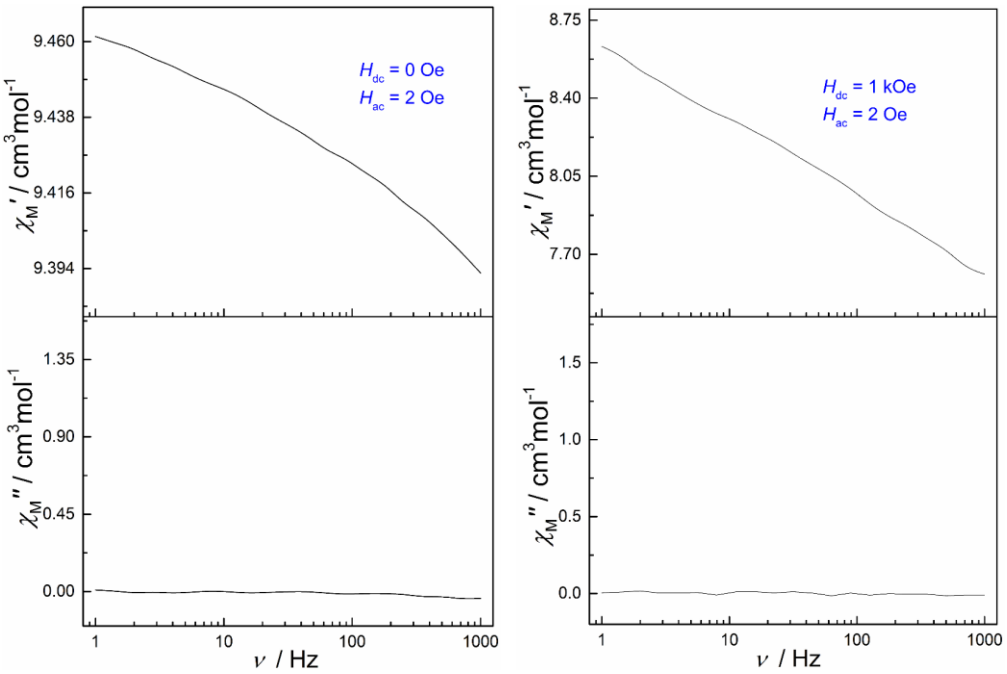

Fig. S11 The real and imaginary components of ac magnetic susceptibility for $\mathbf{5_{Er}}$ at 2 K under zero applied external dc field (left) and a dc field of 1000 Oe (right).

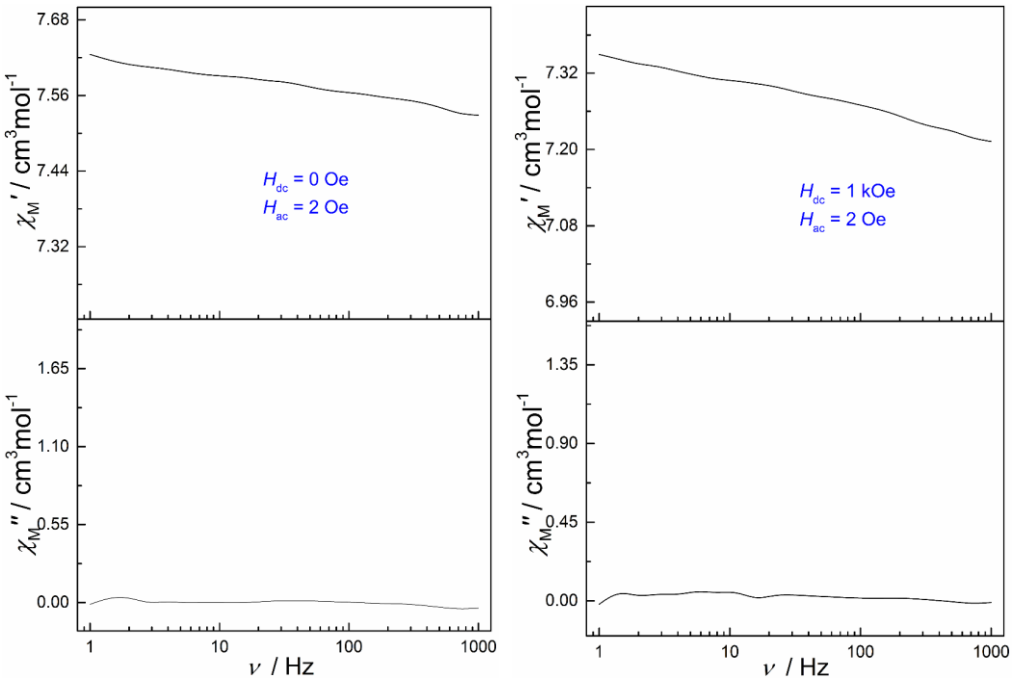

Fig. S12 The real and imaginary components of ac magnetic susceptibility for $\mathbf{6_{Tm}}$ at 2 K under zero applied external dc field (left) and a dc field of 1000 Oe (right).

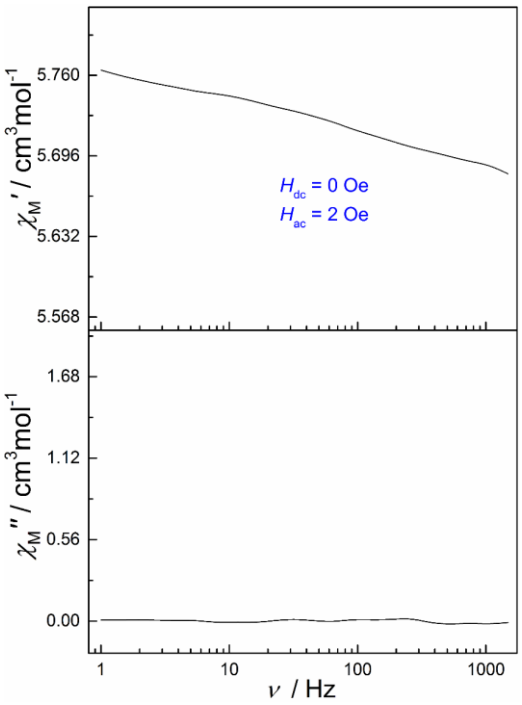

Fig. S13 The real and imaginary components of ac magnetic susceptibility for **7$_{Yb}$** under zero applied external dc field at 2 K.

Table S9 Fitting parameters of Cole-Cole plots of for **7$_{Yb}$** under 1000 Oe applied dc field.

T (K)	χ_0	χ_t	τ	α
1.8	0.11599	1.92010	0.00431	0.16171
2.0	0.10574	1.69948	0.00279	0.13514
2.2	0.10571	1.54446	0.00180	0.10402
2.4	0.09799	1.41033	0.00113	0.08060
2.6	0.09927	1.30300	0.00072	0.05840
2.8	0.10151	1.22460	0.00047	0.04318
3.0	0.11825	1.13885	0.00031	0.01754
3.2	0.11000	1.06819	0.00021	0.01576
3.4	0.10249	1.00752	0.00014	0.00565
3.5	0.04983	0.97950	0.00011	0.03063

Details for calculations

Complete-active-space self-consistent field (CASSCF) calculations on individual Dy^{III}, Ho^{III}, Er^{III}, Tm^{III} and Yb^{III} fragments (see Figure S14 for the calculated model structures of individual Ln^{III}

fragment) extracted from the compounds on the basis of single-crystal X-ray determined geometry have been carried out with MOLCAS 8.2 program package[S1] (see Figure S2 for the complete structures). In the calculation of individual Dy^{III} Ho^{III}, Er^{III}, Tm^{III} and Yb^{III} fragments, the influence of distant Dy^{III} Ho^{III}, Er^{III}, Tm^{III} and Yb^{III} ions were taken into account by the closed-shell La^{III} ab initio embedding model potentials (AIMP; La.ECP.deGraaf.0s.0s.0e-La-(LaMnO3.), respectively.[S2]

The basis sets for all atoms are atomic natural orbitals from the MOLCAS ANO-RCC library: ANO-RCC-VTZP for Dy^{III}, Ho^{III}, Er^{III}, Tm^{III} and Yb^{III} ions, respectively; VTZ for close O; VDZ for distant atoms. The calculations employed the second order Douglas-Kroll-Hess Hamiltonian, where scalar relativistic contractions were taken into account in the basis set and the spin-orbit couplings were handled separately in the restricted active space state interaction (RASSI-SO) procedure. Active electrons in 7 active spaces include all *f* electrons (CAS (9 in 7 for Dy^{III}, 10 in 7 for Ho^{III} ,11 in 7 for Er^{III}, 12 in 7 for Tm^{III}, 13 in 7 for Yb^{III})) in the CASSCF calculations. To exclude all the doubts, we calculated all the roots in the active space. We have mixed the maximum number of spin-free state which was possible with our hardware (all from 21 sextets, 128 from 224 quadruplets and 130 from 490 doublets for individual Dy^{III} fragment; all from 35 septuplets, 150 from 210 triplets and 120 from 196 singlets for individual Ho^{III} fragment; all from 35 quadruplets and all from 112 doublets for individual Er^{III} fragment; all from 21 triplets and all from 68 singlets for individual Tm^{III} fragment; all from 21 sextets, all from 7 doublets for individual Yb^{III} fragment). And then, Single−Aniso[S3] program was used to obtain the ***g*** tensors, energy levels, magnetic axes, *et al.,* based on the above CASSCF/RASSI calculations.

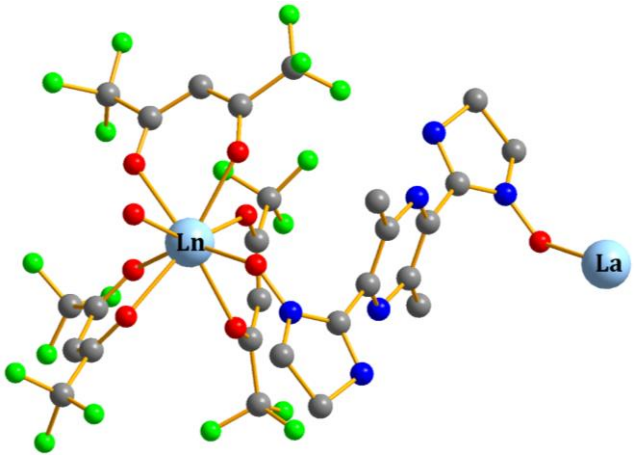

Fig. S14. Calculated model structure of individual Ln^{III} fragment; H atoms are omitted.

Table S10 Calculated energy levels (cm^{-1}), ***g*** (g_x, g_y, g_z) tensors and m_J values of the lowest eight, eight and four Kramers doublets for individual Dy^{III}, Er^{III} and Yb^{III} fragments, respectively, and the lowest nine and seven non–Kramers doublets for individual Ho^{III} and Tm^{III} fragments, respectively.

	Dy^{III}			**Ho^{III}**			**Er^{III}**		
	E/cm^{-1}	***g***	m_J	E/cm^{-1}	***g***	m_J	E/cm^{-1}	***g***	m_J
1	0.0	0.433 1.592 17.263	±15/2	0.0 4.7	0.000 0.000 14.945	±8	0.0	3.804 4.198 11.352	±15/2
2	43.8	2.781 3.655 12.034	±9/2	16.5 30.4	0.000 0.000 11.350	±6	14.3	0.502 3.862 10.759	±1/2
3	78.5	1.593 3.973 12.271	±1/2	51.8 74.5	0.000 0.000 8.768	±2	41.9	0.941 1.260 15.044	±11/2
4	127.2	3.580 4.568 11.322	±5/2	87.5 95.3	0.000 0.000 12.262	±4	82.9	1.452 2.946 8.642	±5/2
5	159.5	0.739 3.647 13.009	±3/2	126.0 146.7	0.000 0.000 10.315	±1	150.5	0.104 3.948 9.208	±13/2
6	194.7	0.971 1.722 15.603	±7/2	181.9 182.8	0.000 0.000 17.334	±7	167.2	0.620 2.452 8.807	±3/2
7	229.2	0.210 0.390 18.507	±11/2	197.4		±0	223.1	2.086 3.491 7.983	±7/2

8	370.9	0.011 0.019 19.781	±13/2	215.0 224.3	0.000 0.000 10.084	±3	247.1	0.261 2.848 12.741	±9/2
9				227.7 231.5	0.000 0.000 11.749	±5			
KDs	**Tm^{III}**			**Yb^{III}**					
	E/cm^{-1}	g	m_J	E/cm^{-1}	g	m_J			
1	0.0 1.5	0.000 0.000 13.708	±6	0.0	0.577 1.153 6.649	±7/2			
2	97.6 101.4	0.000 0.000 13.092	±3	168.0	1.188 1.971 5.887	±5/2			
3	142.6 156.1	0.000 0.000 10.711	±1	248.3	3.221 1.738 0.030	±3/2			
4	173.5 219.0	0.000 0.000 8.029	±4	318.2	1.008 3.016 5.818	±1/2			
5	244.6 247.7	0.000 0.000 5.283	±2						
6	275.1		±0						
7	307.9 316.0	0.000 0.000 11.554	±5						

References

S1 (a) Aquilante, F.; De Vico, L.; Ferré, N.; Ghigo, G.; Malmqvist, P.-Å.; Neogrády, P.; Pedersen, T. B.; Pitonak, M.; Reiher, M.; Roos, B. O.; Serrano-Andrés, L.; Urban, M.; Veryazov, V.; Lindh, R. *J. Comput. Chem*., **2010**, *31*, 224. (b) Veryazov, V.; Widmark, P. -O.; Serrano-Andres, L.; Lindh, R.; Roos, B. O. *Int. J. Quantum Chem*., **2004**, *100*, 626. (c) Karlström, G.; Lindh, R.; Malmqvist, P. -Å.; Roos, B. O.; Ryde, U.; Veryazov, V.; Widmark, P. -O.; Cossi, M.; Schimmelpfennig, B.; Neogr´ady, P.; Seijo, L. *Comput. Mater. Sci*., **2003**, *28*, 222.

S2 Seijo, L.; Barandiarán, Z. *Computational Chemistry: Reviews of Current Trends*; World Scientific, Inc.: Singapore, 1999; pp 455−152.

S3 (a) Chibotaru, L. F.; Ungur, L.; Soncini, A. *Angew. Chem. Int. Ed.*, **2008**, *47*, 4126. (b) Ungur, L.; Van den Heuvel, W.; Chibotaru, L. F. *New J. Chem.*, **2009**, *33*, 1224. (c) Chibotaru, L. F.; Ungur, L.; Aronica, C.; Elmoll, H.; Pilet, G.; Luneau, D. *J. Am. Chem. Soc.*, **2008**, *130*, 12445.